

Optimal Combined Heat and Power Integration of a Micro Gas Turbine Unit in Distributed Energy Generation

Johannes F. Rist^{1*}, Miguel F. Dias^{1†}, Daniel Zelazo[‡], Beni Cukurel[‡], and Michael Palman[‡]

This work considers the optimal combined heat and power (CHP) integration of a micro gas turbine unit in a distributed energy power grid. A detailed thermodynamic cycle analysis is conducted on a representative micro-gas turbine unit with non-constant component efficiencies and recuperator bypass. This model is used to develop an accurate optimization model for solving the economic dispatch problem of integrating the turbine into the grid. The financial benefit and viability of this approach is then examined on a detailed case study using real data on energy demand profiles and electricity tariffs. The optimal schedule follows four fundamental operational modes which are electricity, heat, revenue, and maintenance-cost driven.

I. Introduction

The global demand for energy supply is expected double as compared to the consumption over the last 20 years [1]. Recent studies commissioned by the European Union, the U.S. Energy Information Administration (EIA), and the World Bank all present similar projections of electricity demand increase by roughly 100% from 2000 to 2050 [2–4]. In order to satisfy this demand, the choice of fuel is among the challenges of economic policy, which is significantly dependent on national resources and long-term political interests. According to this EU energy market simulation [4], the future demand for power generation will be exceedingly accommodated by the renewable energy sources, as well as natural gas.

The issue of renewable energy, in particular solar and wind power, presents a specific challenge to the grid infrastructure, since their capacity is not always available. The fluctuations in generation require more re-dispatches by grid operators, and therefore, the renewables alone cannot dominate the future generation infrastructure. Along these lines, the European Union's electricity generation from natural gas has tripled from the 1990s to early 2000s [5]. This trend of continued introduction of natural gas is foreseen in most industrialized countries.

Micro Gas Turbines

The largest increase in the use of natural gas for power generation will primarily be accommodated by the introduction of gas turbines (GT), mainly in combined cycle forms [6].

*J.F. Rist is with the Department of Mechanical Engineering, Technical University of Munich, Germany. johannes.rist@tum.de

†M.F. Dias is with the Department of Aerospace Engineering, Instituto Superior Técnico, Lisbon, Portugal. miguel.f.dias@ist.utl.pt

‡Faculty of Aerospace Engineering, Technion - Israel Institute of Technology, Haifa, Israel. dzelazo@technion.ac.il, beni@cukurel.org, p.michael@campus.technion.ac.il

¹The work was conducted during an internship at the Faculty of Aerospace Engineering, Technion - Israel Institute of Technology, Haifa, Israel.

Moreover, the trend towards deregulation of the electricity supply market vastly enhances the emerging distributed power generation for efficient delivery, as well as towards minimizing transmission and congestion losses [6]. Furthermore, in order to cope with the intermittent availability of the renewable energy sources, it is essential to develop back-up systems [7,8]. There is a particular interest in the potential of technologies such as micro gas turbines (MGT, such as the one portrayed in Figure 1), especially in combined heat and power (CHP) applications and polygeneration systems, where the local main energy consumers become the provider for their electricity, hot water, heating and chill production [5, 9, 10]. Numerous small and efficient gas turbine units can gradually be introduced in order to fulfill the new demands and to replace the larger aging power plants [11]. Consequently, the non-centralized energy infrastructure network becomes more robust, cheaper (gains in distribution losses), safer, and also more versatile.

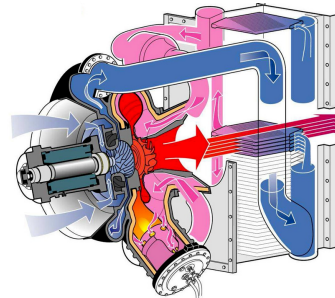


Figure 1: Schematic of a Turbec T100 micro-gas turbine.

Micro-turbines offer additional advantages compared to other technologies for small-scale power generation such as high power-to-weight ratio, relative size (low terrain footprint), reliability (smaller number of moving parts), lower noise and vibrations, multi-fuel capability and lower greenhouse gas emissions [12–14]. Furthermore, the recent developments reflect upon the potential of MGT to serve for polygeneration of energy (CCHP = electricity, heat and chill production). Such systems could theoretically achieve combined thermal efficiencies of above 85% [10], thus reducing running costs and CO₂ emissions. Due to their relative low thermal and mechanical inertia, micro gas turbine units are agile and flexible, capable of short start-up times [15], along with rapid operational transitions between partial and full-load [12–14]. Furthermore, micro gas turbines can be stacked up to create a bank which meets the instantaneous local power demand of their vicinity throughout the day which is extremely relevant for “peak (power) shaving,” reducing the need for large power plants as backup during prime energy consumption intervals.

The technological attractiveness of CHP units is the focus of several recent scientific studies. The work [16] presented an optimization framework for capacity sizing and dispatch planning of CHP units for residential applications, considering economies of scales, CO₂ emissions and annual cost considerations. The interaction between the electrical and natural gas grid for distributed generating units was surveyed in [17]. In this study the load flattening that can be achieved with such units was also addressed. A monthly planning strategy to study long term optimal configurations of CHP units for different types of CHP prime movers, such as biomass and MGT, were addressed in [18]. In [19], an investigation of the necessary number of turbines needed to meet the energy requirements of residential buildings located in several Iranian cities was conducted. The authors argued that given the availability of natural gas in Iran and the proneness of the coun-

try to natural disasters such as earthquakes, on-site CHP systems are a viable solution to increase the reliability of the electrical supply and reduce the dependency from the main grid. Along the same line, an investigation of the viability of CHP units based on MGT in tropical climates was carried out in [20]. The study included economic considerations such as the payback period of installing such systems. A study based on Japanese data, [21], evaluated both the annual costs and CO_2 savings that can be achieved with two types of CHP units, MGTs and Fuel Cells, applied to residential buildings. In this study it was found that fuel cell based CHP unit is the better option. Similarly, [22] presented a method for choosing the best type of CHP unit for residential application in different types of climate.

In all of the above, detailed surveys about CHP benefits such as emission reduction, economic benefits, and partial independence from the main grid were conducted. However the models of the MGTs are often generic and more emphasis is given to the interconnection of the MGT with the other subsystems. This is the starting point of the contributions of this work, detailed in the following subsection.

Motivation and Contribution

The integration of micro-gas turbines into the smart-grid as a polygeneration source can be approached as an economic dispatch (ED) and unit commitment (UC) problem. The ED and UC problems determine an optimal schedule and commitment level for each generating unit in a power system based on a set of constraints, including reserve power, operating parameters, and forecasted loads over a finite time horizon [23–25]. In a smart-grid scenario where power demands can be mitigated locally, a detailed model-based optimization strategy has the potential to offer significant improvements.

While many optimization-based approaches to the operation of the smart-grid have been studied [17, 18, 26], to our knowledge, a focused effort towards optimally integrating a realistic micro-gas turbine with electricity and heat/chill production considerations, along with part load performance, has not been attempted. Furthermore, the base time step for the turbine dynamic modeling usually is in the order of minutes [17], while our more realistic model describes the dynamics of the turbine with a base time step on the order of seconds, allowing for a much more accurate dynamic model.

In this direction, the current work provides a complete solution for the integration of a micro-gas turbine in a smart-grid environment. The main contributions are:

- **Modeling of a Micro Gas Turbine** - A detailed thermodynamic cycle analysis is conducted on a representative MGT unit with non-constant component efficiencies and recuperator bypass. This model provides a detailed MGT performance characterization in a range of operational conditions.
- **Economic Dispatch of an MGT** - An optimization model for the operation of an MGT is provided and it includes characterization of all operating costs and constraints. This model is integrated into an economic dispatch framework by casting the optimization as a *shortest path* problem.
- **Detailed Case Studies** - To demonstrate the advantage of utilizing MGTs for CHP, a detailed simulation is conducted for a residential neighborhood. Analysis of the operational profile of the MGT and its economic benefit is presented.

In addition to an economic analysis of integrating the MGT into the grid, the case studies also revealed that the MGT operates under four distinct modes: *electricity driven*, *heat driven*, *revenue driven*, and *maintenance-cost driven*. Each mode describes the economically optimal way to operate for a given demand profile, fuel costs, and the tariffs. This leads to important insights into the economic dispatch solution and a high-level understanding of how the MGT can best be integrated into the grid.

The organization of this paper is as follows. In Section II, the detailed thermodynamic model of the polygeneration suitable micro gas turbine unit is presented. Section III describes the integration of the MGT model in an economic dispatch framework. The case study demonstrating the advantage of using MGT as a CHP unit in a smart-grid setting are presented in Section IV. Finally, some concluding remarks are offered in Section V.

II. Gas-Turbine Modeling

Although micro gas turbines are exceptionally suitable to meet the on-site needs of distributed power generation, a proper thermodynamic analysis coupled with thermo-economic investigation must be carried out to gain essential information on various available cycle solutions [27]. To provide valid estimation, such studies require accurate microturbine and power distribution system models [28]. To this end, most previous efforts related to the economic dispatch problem simulated the MGT as a dynamic system using the governor model [28–31]. This approach can capture the electro-mechanical response of a generic turbine coupled with a generalized controller, while disregarding the energy conservation laws of individual components (compressor-turbine coupling, combustor performance, and mechanical losses). In the scope of the current work, building upon established tools in the turbomachinery community [32–34], a component based gas turbine model is implemented to fully resolve the steady-state performance of a CHP unit. This allows accurate performance optimization of the MGT in the unit commitment problem.

The Micro-Gas Turbine for Polygeneration

Although there exist a broad range of studies on advanced cycle design and analysis for various applications, due to its compromise in efficiency, reduced mechanical complexity, and imminent applicability, a small single-spool gas turbine engine is considered in a recuperated cycle. The nominal power output of the discussed unit is 100 kW_{el}. The proposed micro-gas turbine model features compact and reliable design that requires low maintenance and operates at competitive efficiency and scale with other energy production technologies such as small reciprocating engines. Comparative CHP gas turbine units exist in the product portfolio of various companies. For example, Capstone C65, Ingersoll Rand PowerWorks 70, Ansaldo Energia (formerly Turbec) AE-T100, Dürr Cleantechnology Compact Power System, and Elliot TA100 all operate in this power range. From publicly available data [35–40], operational parameters of these commercial products are summarized in Table 1.

However, most consumers of these products are rarely interested in operating the unit solely at its design point and typically would like to vary the commitment level based on demand and cost of alternate available energy resources. Therefore, the design point information provided by the manufacturer is insufficient to properly assess the economic value, as the product ideally should also operate under off-design (part load) conditions.

Table 1: Design output parameters of reference MGT units operated in CHP

	Power	Heat	Electrical Efficiency	Cycle Efficiency
Capstone C65	65kW	126kW	29%	up to 90%
I-R PW70	70kW	106kW	28%	70%
AE-T100	100kW	200kW	30%	90%
Durr CPS	100kW	210-520kW	30%	up to 98%
Elliot TA100	100kW	165kW	29%	75%

Hence, a more detailed model of a relevant micro-gas turbine is required to adequately resolve the performance in the entire operational range.

Based on the engine architecture relevant to the industry, the MGT unit we consider consists of a single stage centrifugal compressor, a can-type combustor, a single stage turbine, and a recuperator. In order to accommodate the changing ratio between power and heat generation demand, the recuperator is equipped with a controllable valve which alters the amount of exhaust gasses bypassing the heat exchanger. The schematic of the discussed CHP unit cycle is presented in Figure 2.

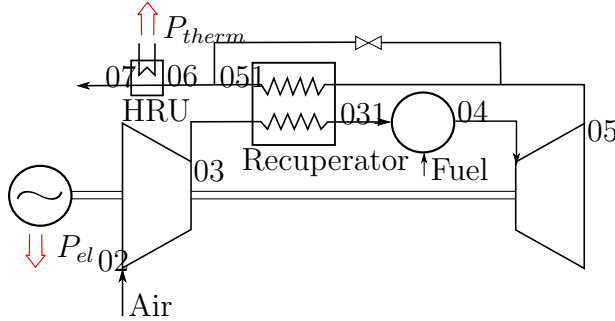


Figure 2: Thermodynamic cycle of a recuperated gas turbine with a heat recovery unit.

The mechanical energy of the shaft is to be extracted by an asynchronous generator, connected to the grid via a voltage and frequency conditioning circuit that includes a rectifier, a DC boost chopper, an inverter bridge, and a filter. Depending upon the geographic location, the output of the power electronics is 400VAC/50Hz or 480VAC/60Hz. Moreover, the system is to include a heat recovery unit (HRU), which is meant to supply the required heat/chill production. However, due to significant differences amongst various applications, the exact mechanical to electrical energy conversion process and the exhaust heat utilization method (via boiler or adsorption chiller) are not modeled in the scope of this investigation.

A. Thermodynamic Equations

Both design and off-design operating parameters of the CHP unit model can be derived from thermodynamic equations that describe the performance of individual non-ideal

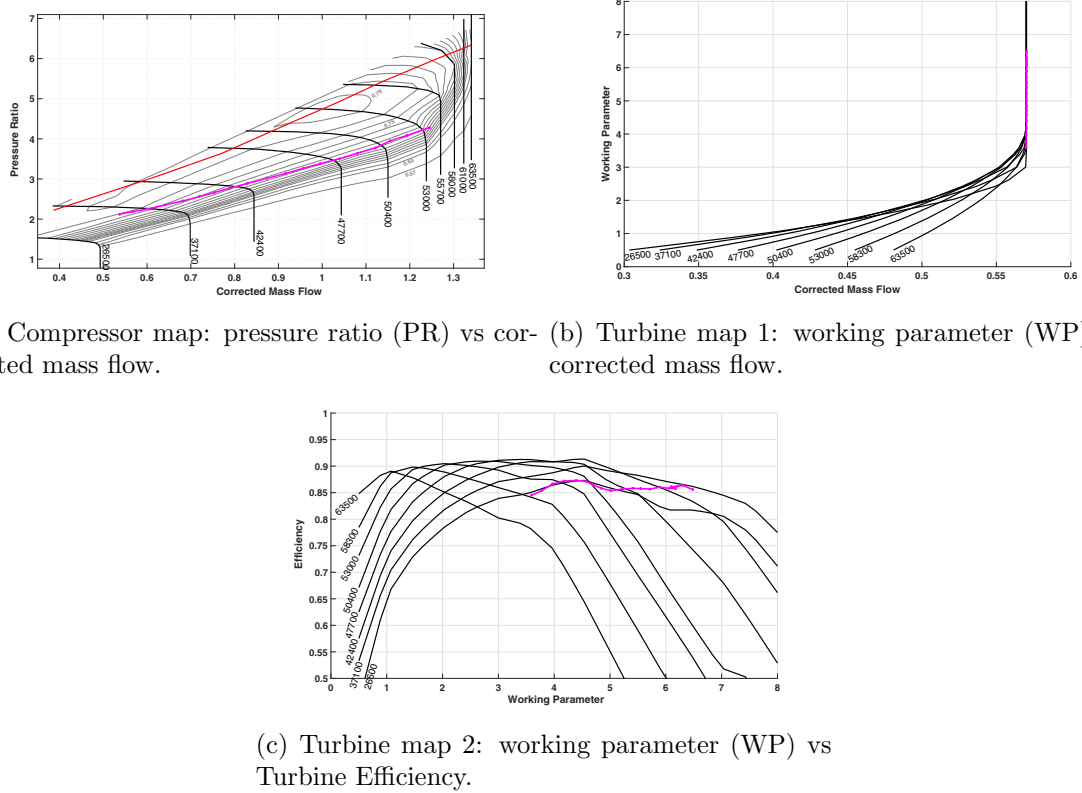


Figure 3: Compressor and turbine maps with an exemplary operating line.

MGT components. The following sections describe the process towards performance evaluation of each element. For proprietary reasons, component characteristics are often not disclosed. Hence, performance parameters of a typical small gas-turbine engine are used throughout the study [41].

Compressor

In general, the behavior of the compressor in the MGT is described by a map which charts the operational envelope in terms of pressure ratio (PR), corrected mass flow rate (\dot{m}_{corr}), corrected rotational speed (N_{corr}), and efficiency (η_C), as depicted in Figure 3(a). The non-dimensional numbers are defined as,

$$\dot{m}_{corr} = \frac{\dot{m} \sqrt{T/T_{ref}}}{P/P_{ref}} \quad (1)$$

$$N_{corr} = \frac{N}{\sqrt{T/T_{ref}}}, \quad (2)$$

where N is the shaft rotational speed, \dot{m} is the mass flow rate through the engine, T is the inlet temperature, P the inlet pressure, and T_{ref} , P_{ref} are standard temperature and pressure reference conditions.

The various speed lines span across the pressure range at their respective efficiency islands. However, in parts of the map, these speed lines can be horizontal or vertical, and render several possible operating points for a given pressure ratio or mass flow requirement. To resolve this ambiguity, auxiliary coordinates (typically known as “beta lines”)

are introduced. Once the appropriate operating point has been selected on the map, the compressor performance is linked to the thermodynamic cycle by

$$\eta_C = \frac{h_{03s} - h_{02}}{h_{03} - h_{02}} \quad (3)$$

$$T_{03} = T_{02} \left(\frac{1}{\eta_c} \left(\left(\frac{P_{03}}{P_{02}} \right)^{\frac{\gamma_c-1}{\gamma_c}} - 1 \right) + 1 \right), \quad (4)$$

which relate the non-ideal work addition to the efficiency and the resultant pressure ratio respectively. The subscripts in the equations refer to the station numbers labeled in Figure 2, and the subscript s denotes the state hypothetically achieved through an isentropic ideal process.

Recuperator

After the pressure rise in the compressor, the temperature of the outgoing flow is further raised by the energy recovered through the recuperator. The efficiency of this process is characterized by

$$\begin{aligned} \eta_{rec} &= \frac{q}{q_{max}} \\ &= \begin{cases} \frac{c_{p,05}\dot{m}_5(T_{05}-T_{051})}{c_{p,03}\dot{m}_3(T_{05}-T_{03})}, & c_{p,03}\dot{m}_3 < c_{p,05}\dot{m}_5 \\ \frac{(T_{05}-T_{051})}{(T_{05}-T_{03})}, & c_{p,05}\dot{m}_5 < c_{p,03}\dot{m}_3 \end{cases}, \end{aligned} \quad (5)$$

which captures the non-ideal heat transfer between the relatively hot and cold gas paths. When electrical power output is required from the unit, the performance of the recuperator highly influences the fuel consumption of the MGT. In contrast, to accommodate high heat or chill demand, the recuperator bypass valve is regulated to retain the exhaust gas temperature. In the scope of this study, the efficiency values are taken from a recuperator of appropriate size [42], the performance data for which is reproduced in Figure 4.

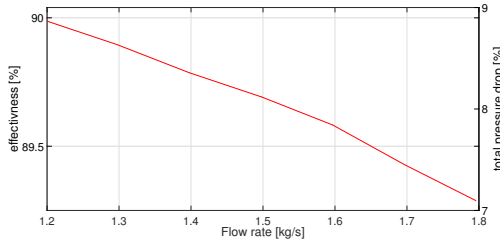


Figure 4: Heat Exchanger Performance.

Combustor

The thermal energy addition of the cycle takes place in the can type combustor, characterized by

$$(\dot{m}_{air} + \dot{m}_f) h_{04} - \dot{m}_{air} h_{031} = \dot{m}_f \dot{Q}_r \eta_b \quad (6)$$

$$\eta_b = 1 - (1 - \eta_{b,dp})(\Omega/\Omega_{dp})^{P_l} \quad (7)$$

$$\Omega = \frac{\dot{m}_{air}}{P_{03}^{1.8} \cdot \exp(T_{03}/300)}, \quad (8)$$

where $\eta_{b,dp} = 0.98$ and $\Omega_{dp} = 0.0160$, $P_l = 1.6$ and $Q_r = 49,736,500 J/kg$. Equation (6) describes the conservation of energy between the incoming air, the calorific value of the fuel burned, and the outgoing combustion products. To calculate the efficiency of this process, an empirical model is introduced in (7). Based on known design point conditions, the off-design efficiency is modeled with reference to combustor loading parameter, (8).

Turbine

The thermal to mechanical energy conversion takes place in the turbine. Two charts are required to describe the turbine operating envelope - the first represents the behavior of the component in terms of the working parameter (WP) as a function of corrected mass flow and corrected rotation speed (Figure 3(b)), and the second relates to the efficiency of the conversion process (Figure 3(c)). For convenience, the definition of the working parameter is provided below,

$$WP = 0.0239 \frac{T_{04} - T_{05}}{T_{04}} \cdot C_p(T_{04}). \quad (9)$$

Portraying the non-ideal nature of the expansion process, the following relations can be written

$$\eta_T = \frac{h_{04} - h_{04}}{h_{04} - h_{05s}} \quad (10)$$

$$\frac{T_{04} - T_{05}}{T_{04}} = \eta_t \left(1 - \left(\frac{P_{04}}{P_{05}} \right)^{-\frac{\gamma_h-1}{\gamma_h}} \right) \quad (11)$$

In the following, the energy extracted by the turbine with respect to the energy consumed by the compressor and the generated electrical power are balanced as

$$\overbrace{\dot{m}_{air} (h_{03} - h_{02})}^{P_{compressor}} + P_{gen} = \eta_m (\dot{m}_{air} + \dot{m}_f) (h_{04} - h_{05}). \quad (12)$$

Heat Recovery Unit

Passing through the hot side of the recuperator, the last station of this cycle is the Heat Recovery Unit (HRU). Providing a heat (or indirectly a chill) source for the consumer, this component extracts heat from the exhaust gasses. After the flow of recuperator exit and the bypass duct undergo flow mixing, HRU essentially acts as an additional heat exchanger, and therefore its performance model is synonymous with the recuperator,

$$h_{06} = h_{051} \cdot (1 - \beta) + h_{05} \cdot \beta \quad (13)$$

$$P_{heat} = \eta_{HRU} \dot{m}_5 \cdot (h_{06} - h_{07}). \quad (14)$$

The outlet temperature after the HRU is typically higher than 100°C [43], and therefore the outlet enthalpy h_{07} is calculated for this constant value.

In the cooling mode of operation, the absorption chiller is directly driven by the waste heat extracted from the heat recovery unit. Detailed modeling of absorption chiller is highly complex [44] and beyond the scope of this work. Therefore, an absorption chiller, with constant performance, is considered. The efficiency of this process is described by the coefficient of performance (COP),

$$COP = \frac{\text{Cooling Power}}{\text{Heating Power}} \quad (15)$$

which is typically assumed to be 0.7 for single-stage units [45, 46]. Thereby, with the COP formulation, the demand for chill is related with the demand for waste heat.

B. Numerical Modeling of Micro-Gas Turbine

Solving the equations developed in Section A can be used to generate the steady-state relationship between the MGT shaft speed, bypass valve position, and fuel consumption. This directly relates to the cost of locally producing electricity and heat at a desired level which can be used to optimize its operation when integrated into the power grid.

Although the thermodynamic behavior of various MGT components are well defined, the solution methodology for finding their steady-state relations can be non-trivial. In the scope of this work, an approach based on NASA's DYNGEN algorithm [32] is used; the flow chart is presented in Figure 5. On a similar scale MGT, the high level of accuracy of this technique was prior demonstrated in [47]. For a given shaft rotational speed and bypass valve position, the location on the compressor beta line is initially assumed. Then, the mass flow, pressure ratio and efficiency are extracted from the compressor map, setting T_{03} . The temperature downstream of the combustor (T_{04}) and the recuperator (T_{031}) are guessed sequentially to initiate the two inner-loops of the compressor-turbine matching. The required fuel flow, which matches the prescribed T_{04} , is subsequently calculated to find T_{05} . These values are used to extrapolate mass flow, pressure ratio and efficiency from the turbine maps. At first, the mass flow through the turbine is calculated and T_{031} is updated until convergence. In following, the fuel mass flow is iterated upon. Finally, the initial beta line guess is revised by the calculation of the HRU exhaust pressure. When the algorithm fully converges, a steady state solution is reached, which relates the fuel mass flow rate, electrical power, and heat output to the shaft rotational speed and bypass valve position.

C. Cycle Parameters for Operational Optimization

In order to optimize the MGT cycle during its operation, two input parameters (shaft speed and bypass valve position) are selected and simulated to yield a number of solution states (electrical power, heat output, and fuel mass flow). For this study, we considered 9 discrete speed levels (from 66% to 100% of rated rpm) and 5 discrete bypass settings (from 0% to 80%). The discrete parameter maps of these steady-state relations are presented in Figure 6.

The thermodynamic performance of the MGT is characterized in electrical power and heat output domains ranging between $30kW_{el} - 110kW_{el}$ and $57kW - 452kW$ respectively; see Figures 6(a), 6(b), 6(c). For a closed bypass valve, while the heat to power output ratio is between 1.4-1.8, this range reaches values of 4.5-7.5 at maximal 80% bypassing. Moreover, providing a measure for CHP unit performance, the heat and electricity generation efficiencies are represented in Figure 6(d) and 6(e) respectively. For a fixed

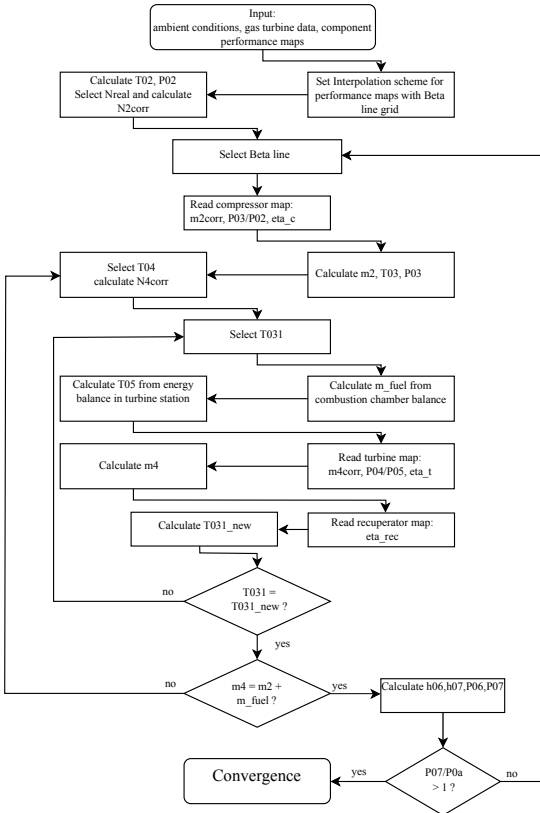


Figure 5: Numerical simulation model flowchart of the recuperated MGT.

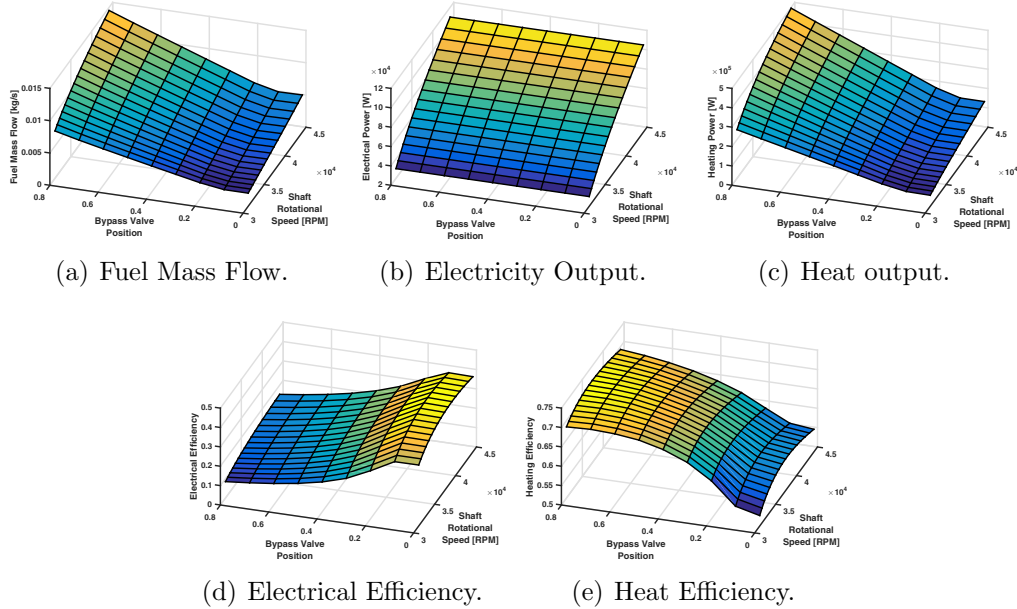


Figure 6: Solution grid over the states of the gas turbine model.

electrical output, when the recuperator bypass valve is opened, the heat output expectedly increases, along with the heat generation efficiency. Although the rotational speed of the shaft is retained throughout this process, due to the increase in fuel mass flow rate

that satisfies the energy balance, the electrical efficiency drops. Across the operating conditions in the range of 0%-80% bypassing, the electricity and heat generation efficiencies vary between 41%-9% and 52%-71% respectively. These values are consistent with the units existing in the market - see Table 1.

III. Economic Dispatch for Micro-Gas Turbines

The detailed modeling of the micro-gas turbine allows for realistically considering its integration into a power generation system. In this direction, we apply the model developed in Section II to an optimal economic dispatch framework in a smart-grid environment. In the following, we present a detailed optimization model of the MGT and the economic dispatch problem.

A. Optimization Model for Micro-Gas Turbines

The economic dispatch (ED) problem is the short-term optimal determination of generation unit outputs aimed at satisfying the system load while minimizing the overall cost. In this work, the operation of a micro-gas turbine as a CHP unit is considered, and thus the ED problem is to determine optimal schedules for both the power output and heat generation of the MGT that minimizes the overall cost to the user. This includes costs incurred from the operation of the MGT (mostly attributed to fuel), in addition to the cost of purchasing power and heat from the utility in the event that the turbine is not economically feasible to operate, or when it can not completely satisfy the demands.

We denote by $x_{GT}(t)$ the MGT state corresponding to a given power and heat output level at time t . As discussed in Section C and summarized in Figure 6, the generator power and heat output are directly related to the turbine speed and bypass valve setting. For generality, we assume the turbine can operate at s fixed speed levels - each speed level is denoted as p_i , for $i = 1, \dots, s$. The amount of heat the turbine can output is a function of the bypass valve that takes a value between 0 (closed) and 1 (completely open). This is denoted by the variable h_j , for $j = 1, \dots, v$ with $h_1 = 0$ and $h_v = 1$. Thus, the complete state of the turbine can be characterized by the pair $x_{GT}(t) = (p_i(t), h_j(t))$.

The MGT speed and valve setting can be mapped directly to the fuel mass flow, as shown in Figure 6(a). Thus, the cost of operating the generator at a given state is a function of the cost of fuel and the function $C_{GT}(x_{GT}(t))$ is the fuel cost for operating the turbine at that level.

Similarly, the variables $x_{UT}^P(t)$ and $x_{UT}^H(t)$ denote the power and heat commitment purchased from the utility^a at time t with cost functions $C_{UT}^P(x_{UT}^P(t))$ and $C_{UT}^H(x_{UT}^H(t))$ respectively. The ED cost function for a finite time horizon of T units can be expressed as

$$J(x_{GT}, x_{UT}^P, x_{UT}^H) = \sum_{t=1}^T (C_{GT}(x_{GT}(t)) + C_{UT}^P(x_{UT}^P(t)) + C_{UT}^H(x_{UT}^H(t))). \quad (16)$$

The minimization of the cost function (16) is subject to several restrictions capturing both the power and heat balance of the system, and the operational constraints of the

^aHeat is not directly sold by the utility, but can be modeled as an additional fuel or electricity cost. This is discussed in more detail in Section 2.

generator. The energy balance equations are the thermodynamic and power restrictions of the microgrid operation. We denote the nominal demand for power and heat at time t with the variables $P(t)$ and $H(t)$. For the turbine state $x_{GT}(t)$, there is a corresponding power and heat output, denoted by $P_{GT}(x_{GT}(t))$ and $H_{GT}(x_{GT}(t))$ respectively (Figures 6(b) and 6(c)). Thus, the energy balance can be expressed as

$$P_{GT}(x_{GT}(t)) + x_{UT}^P(t) = P(t), \quad t = 1, \dots, T, \quad (17)$$

$$H_{GT}(x_{GT}(t)) + x_{UT}^H(t) = H(t), \quad t = 1, \dots, T. \quad (18)$$

In the absence of any additional constraints, the ED problem aims to minimize (16) subject to the energy balance constraints (17) and (18).

While one may consider purchasing power and heat from the utility in an instantaneous manner, extracting heat and power from the MGT implicitly induces dynamics, which we develop here. Recalling that the time constant corresponding to changes in the MGT state are fast relative to the operating horizon, this economic dispatch problem considers transition from one MGT state to another via steady-state operational behavior only. Along these lines, a control variable, $u_{GT}(t)$, which is used to determine how the turbine should change states at each time-step, is introduced. This leads to a discrete-time dynamical system, represented below as,

$$x_{GT}(t + c\Delta T) = f_{GT}(x_{GT}(t), u_{GT}(t)), \quad (19)$$

where a fixed step-size of ΔT seconds is assumed. As we are concerned with only the steady-state operation, the step-size should be chosen to be faster than the transient dynamics, but short enough to capture the scheduling objective for the ED problem. The constant c is used to emphasize that certain transitions may require multiple time-steps to complete.^b

The form of the function f_{GT} , therefore, captures both the allowable state transitions of the MGT, and the number of time steps each transition requires. As shown in [48], dynamics expressed in this form can be represented by a state-transition diagram leading to a qualitative description of the dynamics (19). As an illustrative example, consider the steady-state operation of the turbine with bypass level fixed to h_1 . The state-transition diagram representing allowable power level transitions is depicted in Figure 7. It can be observed in this example that increasing the speed level requires two time-steps (i.e., $c = 2$), while decreasing requires a single time-step (i.e., $c = 1$). Furthermore, speed levels must be increased or decreased sequentially (for example, the generator can not transition from state (p_1, h_1) to (p_3, h_1) without passing through (p_2, h_1)). However, it is possible to change both the speed level and the bypass valve setting in the same time step, provided that the requirement of sequential speed changes are respected. Note that Figure 7 represents only a portion of the complete state-transition diagram, which contains $p_s h_v$ possible states at each time step. The exact number of time steps required for changing states depends on the step-size ΔT .

The MGT also requires special start-up and shut-down procedures. When the generator is in the ‘off’ state (corresponding to $x_{GT} = (0, 0)$), it must be ramped up to full power (i.e., p_s with any bypass valve setting). Furthermore, the transition from the ‘off’ state to the first online state takes T_{SU} minutes. Hence, if increasing the speed level takes two time-steps, the complete start-up procedure takes $SU_t = T_{SU}/\Delta T + 2\Delta T \cdot s$

^bFurthermore, the constant is a function of the current generator state and the control.

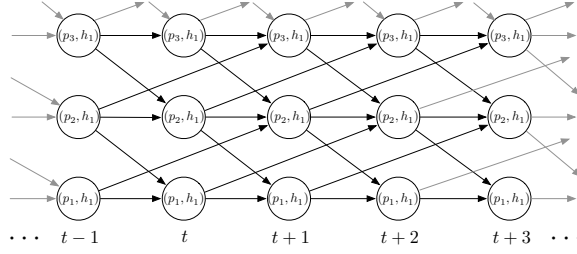


Figure 7: A portion of the transition graph of MGT during online operation.

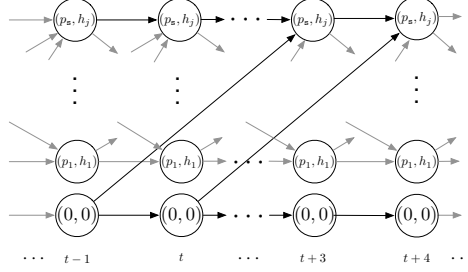


Figure 8: Portion of the start-up transition diagram for MGT.

time steps. Similarly, the generator can only be shut down from the state (p_1, h_1) and requires T_{sd} units of time to be completely off-line. Figure 8 depicts the transition graph highlighting the beginning of a start-up procedure where T_{SU} corresponds to 4 time steps. We assume for this study a start-up time for the MGT of 2 minutes, and a shut-down time of 3 minutes [15].

Using this state-transition graph representation, it is possible to embed in the generation cost a *transition* cost that models the added cost for changing states. We assume that the generation cost, $C_{GT}(x_{GT}(t), u_{GT}(t))$, includes these transition costs. This allows to completely characterize the economic dispatch problem for operating the MGT in a smart-grid environment as the optimization problem

$$\begin{aligned} \min_{x_{GT}, u_{GT}, x_{UT}^P, x_{UT}^H} \quad & J(x_{GT}, u_{GT}, x_{UT}^P, x_{UT}^H) \\ \text{subject to} \quad & x_{GT}(t + c\Delta T) = f_{GT}(x_{GT}(t), u_{GT}(t)), \\ & P_{GT}(x_{GT}(t)) + (x_{UT}^P(t) - P(t)) = 0, \\ & H_{GT}(x_{GT}(t)) + (x_{UT}^H(t) - H(t)) = 0, \\ & x_{GT}(t) \in \{(p_i(t), h_j(t)), i = 1, \dots, s, j = 1, \dots, v\} \\ & x_{UT}^P(t) \geq 0, x_{UT}^H(t) \geq 0, t = 1, \dots, T. \end{aligned} \quad (20)$$

In the next subsection, solution methods for (20) will be discussed.

B. Solution Methods - A Shortest Path Approach

The general form of the optimization problem in (20) falls under the class of mixed-integer programming (MIP). The description of the dynamics using a state-transition graph allows for employing the shortest path algorithm to solve the problem [48, 49]. As shown in Section A, each node in the graph represents the operating state of the MGT (the state $x_{GT}(t)$) at a given time t . Thus, if we operate for T units of time with

time-steps of ΔT , the complete network must contain $p_s h_v T / \Delta T$ nodes. The edges of the graph are determined by the MGT discretized dynamics (19). Hence the graph can be constructed independently of the cost assignment. Furthermore, given that the graph evolves forward in time, it can be categorized as a *directed acyclic graph* (DAG), which leads to efficient shortest path algorithms [50, 51].

The main challenge for employing the shortest path algorithm is to accurately map the cost functions, described on the nodes of the graph, to appropriate transition costs assigned to each edge. Furthermore, the cost structure must embed the enforcement of the energy balance constraints. In this direction, recall that the energy balance constraints (17) and (18) are always satisfied - power and heat is purchased from the utility whenever the MGT does not meet the demand. Thus, each generator state $x_{GT}(t)$ determines the amount of power and heat to be purchased from the utility explicitly (the costs $C_{UT}^P(x_{UT}^P(t))$ and $C_{UT}^H(x_{UT}^H(t))$). To compute the edge weight between adjacent nodes, we assume the cost to be the average cost between the adjacent edges. In this direction, we denote by $\bar{P}(t, t + c\Delta t)$ and $\bar{H}(t, t + c\Delta t)$ as the average power and heat demand over the time interval t and $t + c\Delta t$. The MGT cost associated with the edge is computed as

$$\bar{C}_{GT}(t, t + c\Delta T) = c\Delta T \frac{C_{GT}(x_{GT}(t)) + C_{GT}(x_{GT}(t + c\Delta T))}{2},$$

and the average power and heat supplied by the MGT is

$$\begin{aligned}\bar{P}_{GT}(t, t + c\Delta T) &= c\Delta T \frac{P_{GT}(x_{GT}(t)) + P_{GT}(x_{GT}(t + c\Delta T))}{2} \\ \bar{H}_{GT}(t, t + c\Delta T) &= c\Delta T \frac{H_{GT}(x_{GT}(t)) + H_{GT}(x_{GT}(t + c\Delta T))}{2}.\end{aligned}$$

The cost of the power and heat purchased from the utility can then be computed as

$$\begin{aligned}\bar{C}_{UT}^P(t, t + c\Delta T) &= c\Delta T C_{UT}^P(\bar{P}(t, t + c\Delta t) - \bar{P}_{GT}(t, t + c\Delta T)) \\ \bar{C}_{UT}^H(t, t + c\Delta T) &= c\Delta T C_{UT}^H(\bar{H}(t, t + c\Delta t) - \bar{H}_{GT}(t, t + c\Delta T)).\end{aligned}$$

Note that if $\bar{H}(t, t + c\Delta t) - \bar{H}_{GT}(t, t + c\Delta T) < 0$, the excess heat is dumped into the atmosphere and the cost is 0. In summary, the edge transition cost can be expressed as

$$\begin{aligned}e(x_{GT}(t), x_{GT}(t + 1)) &= \bar{C}_{GT}(t, t + c\Delta T) + \\ &\quad \bar{C}_{UT}^P(t, t + c\Delta T) + \bar{C}_{UT}^H(t, t + c\Delta T).\end{aligned}\tag{21}$$

In addition to the costs described above, there is a cost associated with the start-up and shut-down of the unit. Considering that the price of the gas turbine engine is roughly \$75,000, and based on typical low cycle fatigue life of 10000 cycles [52], it is possible to estimate the cost of each shutdown and startup as \$3.75 each. During the startup and shutdown procedures, we assume the MGT is offline for the entire duration, and thus all electricity and heat much be purchased from the utility, contributing to the edge cost.

To complete the construction of the graph, artificial “start” and “end” nodes are added; these states are unrestricted and do not represent a constraint for the optimization. Thus, we allow the optimization to begin at any generator state without incurring a cost. The above modeling provides a methodical way to construct the directed acyclic graph. In this scenario, the shortest path solution would correspond precisely to the optimal operating schedule of the MGT.

IV. Case Study - A Residential Neighborhood

To demonstrate the benefit of integrating a single micro gas turbine into the electricity market, we provide a detailed case study on a residential building neighborhood. In the following, we present a detailed model of the demand profiles and electricity tariffs. We then solve the economic dispatch problem using the formulation developed in Section III. Finally, we present an economic analysis of the optimal operation strategy.

A. Demand and Environment Modeling

In this section, the models for energy demand and load profiles are presented. Moreover, a thorough discussion on the electricity tariffs used to define the cost structure is included.

1. Energy Demand and Load Profiles

For the entire year of 2004, the U.S. Department of Energy published the demand profiles of 16 commercial and 3 residential reference buildings, separated by source (electricity, gas) and consumption type (e.g., lights, facility, heating, cooling) [53, 54]. Based on the available data, the effectiveness of employing a MGT as a CHP unit is considered for a residential neighborhood

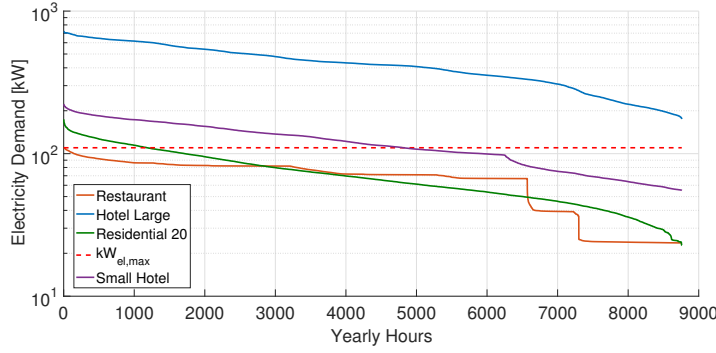
- **A residential building with high load:** a neighbourhood consisting of 20 apartment buildings, on which the residential electricity tariff applies.

In the scope of this work, towards simplicity, the demand is categorized as general electrical power and heat (cooling is related to heat through the absorption chiller coefficient of performance). A histogram of the annual electricity load profiles of four different reference buildings is given in Figure 9(a) for comparison. The red dashed line marks the maximum electricity output that can be generated by the CHP unit considered in this investigation. Similarly, heat load curves are presented in Figure 9(b), where the two horizontal red lines show the minimum (0% bypassing) and maximum (80% bypassing) heat production at maximal electricity output. The yearly hours portrayed are not consecutive, but rather a representation of frequency for a demand level above the designated value. It can be seen that for larger buildings (such as a large hotel), the maximum electrical output of a single unit is not sufficient to ever meet the entire demand, whereas the heat output is at times only partially fulfilled by the CHP. Contrasting this to the case of the restaurant, the heat and electrical capacity of the MGT consistently surpasses the need. For the other building types, the heat and electricity supplied by the MGT should be determined according to time-varying demand level and the associated cost with respect to the utility.

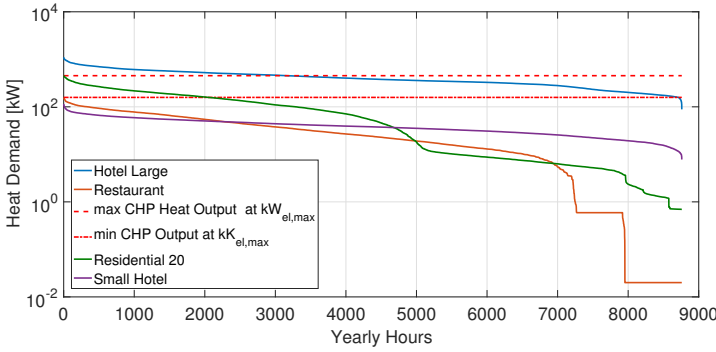
2. Electricity and Heat Tariffs

In general, many different electricity tariffs exist; they reward certain behavior while penalizing divergent conduct. In this work, aggregation of the electricity tariffs are modeled according to the framework proposed in [55]. As described in [56, 57], the tariffs comprise three cost components: fixed costs (FC), fixed pricing of energy (FPE), and demand charging (DC) . We denote by $g(\Delta P(t))$ the function that defines the cost of electricity,

$$g(\Delta P(t)) = \begin{cases} A \cdot \Delta T \cdot \Delta P(t) + B + C, & \Delta P(t) \geq 0 \\ A \cdot \Delta T \cdot \Delta P(t), & \Delta P(t) < 0 \end{cases}, \quad (22)$$



(a) Power demand histogram.



(b) Heat demand histogram.

Figure 9: Histogram of annually demand profiles for different microgrid consumers. Output limitations of the CHP unit are highlighted.

where

$$\Delta P(t) = P(t) - P_{GT}(x_{GT}(t))$$

and ΔT is the time step increment (in seconds) we use to schedule the MGT operation. In (22), A represents the (linear) energy charge (in \$/kWh), B the demand charge (in \$), and C is service and metering charge (in \$) - calculated per day of utilization .

The demand charge, B , is the cost associated with providing service during peak demand periods. It is used to penalize the power consumption in commercial buildings based on the highest average kW maintained during any 15-minute interval within the billing cycle [58]. The charge B is divided into two different components, the peak demand charge (PDC), and the intermediate demand charge (IDC), and is defined as,

$$B = \begin{cases} \text{summer} \\ \frac{1}{30} \left(\text{PDC} \cdot \max_{t \in t_{\text{peak}}} (P(t)) + \text{IDC} \cdot \max_{t \in t_{\text{int}}} (P(t)) \right), \\ \text{winter} \\ \frac{1}{30} \text{IDC} \cdot \max_{t \in t_{\text{int}}} (P(t)) \end{cases}, \quad (23)$$

where t_{peak} represents the peak hours and t_{int} the intermediate hours (see Table 3). Usually the billing cycle is a full month, but in this study, its contribution to a single day is considered; therefore, the value obtained is divided by 30 (average month duration) to yield the daily contribution to the cost.

As discussed in Section III, a cost must be assigned to each transition edge modeling the operation of the MGT in the economic dispatch problem. Based on the tariff model (22), only the linear energy charge, A , is used to compute the the cost of an edge in (21). For the purpose of this study, we apply the fixed usage costs B and C *a posteriori* to provide a more accurate economic analysis.

The rates A, B, C , of each building type are different and vary according to the time of the day. In this work, pricing data from PSEG Long Island New York is used [56, 57], summarized in Table 2. The pricing is based on Time-of-Use and fixed costs for all buildings (A and C in (22)), in addition to demand charge applied only to commercial medium and tall buildings (B in (22)). Within this structure, the cost of time-of-use and demand charges are regulated at different time intervals. The *peak hours* refer to time periods with high load on the grid, whereas low load hours (typically during the evenings) are denoted as *off-peak*; and hours between these times with moderate demand, are evaluated on an *intermediate* pricing level. The exact definition of peak, intermediate, and off peak hours vary depending on the building type and the season. Splitting the year into two seasons (summer/winter), *summer* is defined to be the time period between June 1st and September 30th. A complete definition of these peak, intermediate, and off peak intervals is given in Table 3. Therein, it can be seen that the peak pricing only applies to the summer period.

Table 2: Electricity tariff rates

		Off Peak	Intermediate	Peak
Commercial medium (restaurant, small hotel)	A	\$/kWh 0.0273	\$/kWh 0.0412	\$/kWh 0.0444
	PDC/IDC	-	\$/kW 3.9	\$/kW 45.48
	C		\$ 1.68	
Commercial tall (large hotel)	A	\$/kWh 0.0291	\$/kWh 0.0435	\$/kWh 0.0543
	PDC/IDC	-	\$/kW 5.34	\$/kW 22.44
	C		\$ 10.16	
Residential (residential neighbourhood)	A	\$/kWh 0.0442	\$/kWh 0.0866	\$/kWh 0.2461
	PDC/IDC	-	-	-
	C		\$ 1.65	

In addition to electricity, the energy source for heat/chill can also be obtained from the utility to achieve energy balance between the demand and supply. As most consumers use a boiler to satisfy their heat demand, we model the heating cost with the price of natural gas. The boiler can be modeled by the grouping of a combustor with a heat recovery unit, described by (6) and (14) respectively. Combining the two previous equations, the heating power of the boiler can be related to the fuel flow rate as,

$$\frac{P_{heat}}{m_f} = \eta_{HRU} (AFR + 1) \left(\frac{\dot{Q}_r \eta_b + AFR \cdot h_{amb}}{AFR + 1} - h_{100^\circ C} \right), \quad (24)$$

where h_{amb} is the specific enthalpy of ambient temperature air at the combustor inlet, and $h_{100^\circ C}$ represents the specific enthalpy of exhaust gasses (considered to be at $100^\circ C$). The air to fuel ratio (AFR) is assumed to be constant and for natural gas $AFR = 17.2 \cdot 1.2 = 20.64$, where 17.2 is the stoichiometric ratio for methane-air mixture and the factor 1.2 is associated with the typical 20% lean burn.

For the chill production, buildings typically employ either conventional electric motor-powered chillers or gas-fired absorption cycle systems. The latter reduces the demand on

Table 3: Definition of off peak, intermediate and peak periods for both seasons

		Summer	Winter
Commercial medium	Off Peak	23:00-07:00	23:00-07:00
	Intermediate	07:00-12:00 & 20:00-23:00	07:00-23:00
	Peak	12:00-20:00	-
Commercial tall	Off Peak	00:00-07:00	00:00-07:00
	Intermediate	07:00-10:00 & 22:00-24:00	07:00-24:00
	Peak	10:00-22:00	-
Residential	Off Peak	20:00-10:00	20:00-10:00
	Intermediate	-	10:00-20:00
	Peak	10:00-20:00	-

the grid which can help alleviate the high electric costs in the summer when the peak hour charges apply. In order to provide an impartial assessment to the value of the MGT with respect to the utility, the consumers are assumed to be using absorption chillers to satisfy their cooling demands. This implies that the chill demand can be related to the heat demand by the absorption chiller's COP factor (0.7). Thereby, the cost of purchasing heating and cooling from the utility can be lumped into the price of natural gas.

3. Net Metering

As the production capacity of the micro CHP unit is finite and predetermined, the energy balance between the local demand, the CHP output, and the utility commitment must be met, according to (17)-(18). Thus, depending on factors including the demand level and cost of fuel, power can be either bought from or sold to the utility.

One of the common approaches for regulating and accounting excess electricity (i.e., the difference between generated power and the demand) is known as *net metering* [59]. The bi-directional electricity flow in and out of the grid is typically accounted at the same tariff rate. Hence, net metering values excess power at retail cost. This is captured in (22) such that when the generation cost is negative ($\Delta P(t) < 0$) and the electricity is sold back to the grid.

As heat is not a directly tradable quantity, there is no mechanism equivalent to net metering for the transfer of thermal energy. Thus, any excess heat generated by the CHP is simply released to the environment.

B. Economic Dispatch

For the case study considered in this work, we take $s = 9$ speed levels for the turbine, $v = 5$ valve settings (from 0% to 80 %), and a time step of $\Delta T = 15\text{sec}$. Thus, at each time step, the MGT can assume 1 of $sv + 1 = 46$ states, which includes one offline state. For a 24 hour horizon, the resulting shortest path graph contains on the order of 1×10^6 edges.

In the examples to follow, we consider a fixed gas price of $\$7.74/1000\text{ft}^3$. This value is the reference cost on October 2015 [60], and it can be related to cost of fuel mass flow

rate through the density of methane, $\rho_{CH_4} = 0.68 \text{ kg/m}^3$.

In order to demonstrate the typical operational behaviour of the system, the economic dispatch problem is solved over three reference days, which represent typical seasonal variations: a winter day (January 10th), a mid-season day (April 10th), and a summer day (July 10th). Each of these days contribute to the aggregate demand data presented in Figure 9. Given that electrical companies usually define two different rating periods [56, 57], *summer* (June 1st - September 30th) and *winter* (October 1st - May 31st), these exemplary days are sufficient to accurately depict the trends for the whole year. Furthermore, the actual demand data is only available in an hourly basis. In order to form a more realistic dynamic demand profile, the data is smoothed with a moving average filter (with a time window of 5 minutes) to ensure more gradual transitions of the demand.

Residential Neighborhood

For the residential neighborhood scenario, the solution of the CHP unit economic dispatch are presented in Figures 10(a)-10(f). On the reference winter day, the CHP unit operates at constant heat (193kW) and maximum electricity production (110kW). Between 17h-22h, when the power demand surpasses the MGT capacity, additional electricity is bought from the utility. In all other time intervals, the excess electricity is sold to the grid according to net metering procedure. It is interesting to note that the heat production is kept at a constant level (at 20% bypass) throughout the day, and it is more economical to purchase additional heat from the utility when needed. This is in part associated with the relatively coarse bypass valve grid employed in the optimization (see Remark ??).

During the typical spring day, the MGT unit behavior presents a unique operational schedule which is *revenue driven*. In the intermediate tariff hours of the day (10h - 20h), the CHP unit operates at an electricity and heat production level significantly beyond the consumer demand, selling all the excess electricity to the grid while dumping the excess heat to the atmosphere (see Figures 10(b) and 10(e)). Therefore, the optimal solution is to take advantage of the higher electricity rates during this period to increase revenue. In fact, in order to increase the electrical efficiency, the bypass valve is set at 0% and the associated heat commitment level is the lowest possible for the chosen speed setting. In this particular circumstance, the MGT can clearly produce electricity at a lower per unit cost than the utility. In the late evening from 20h-24h, when the utility costs are low, the CHP operates at its lowest possible power and heat state instead of shutting down (maintenance driven). For the same day, in the off-peak tariff hours (24h-7h), the CHP unit supplies the entire heat demand at 0% bypass and varying speed levels (heat driven behavior). The ensuing excess electricity is sold back to the grid. Lastly, from 7h-10h, the commitment level of the CHP changes directly correlated with the electricity demand, varying the speed of the engine at 0% bypass level in the most thermodynamically efficient condition (electricity driven).

During the summer day, the electricity is at peak rate between 10h-20h, which increases the economic advantage of production by the MGT. In fact, between 10h-11h, the unit produces 110kW electricity at 0% bypass (greater than the demand) and sells the surplus back to the grid (revenue driven). From 12h - 20h, the power demand exceeds the capacity of the MGT, and the additional requirements are supplied by the utility. However, this time period is not entirely electricity driven. Between 16h-17h, with the increasing heat demand, the bypass valve position is adjusted to 20% in order to produce

more heat at the same electricity production rate (100% speed). Hence, the optimization finds economic advantage in producing heat through the MGT at the expense of augmented fuel consumption. In the off-peak hours of 20h-24h and 07h-10h, the trends are heat driven due to lowered price of electricity. Once again, in the early hours of the day between 24h - 07h, the MGT operates in its minimum electricity and heat production state, instead of shutting down (maintenance driven). In this time period, it is more economical to fulfill the additional electricity demand from the network.

Throughout the various seasons and times of day, the residential neighborhood presents differing optimal commitment trends associated with heat, electricity, revenue, and maintenance -cost driven operation. In contrast to other consumers of energy, the increased diversity in the neighborhood's economic dispatch mode is heavily based on the variations in the ratio between the power to heat demand, which fluctuates between 0.2-6. In contrast, the heat to power demand ratio of the restaurant varies between roughly 0 - 1.5 throughout the year. This increased range of this ratio has strong influence on the optimization strategies.

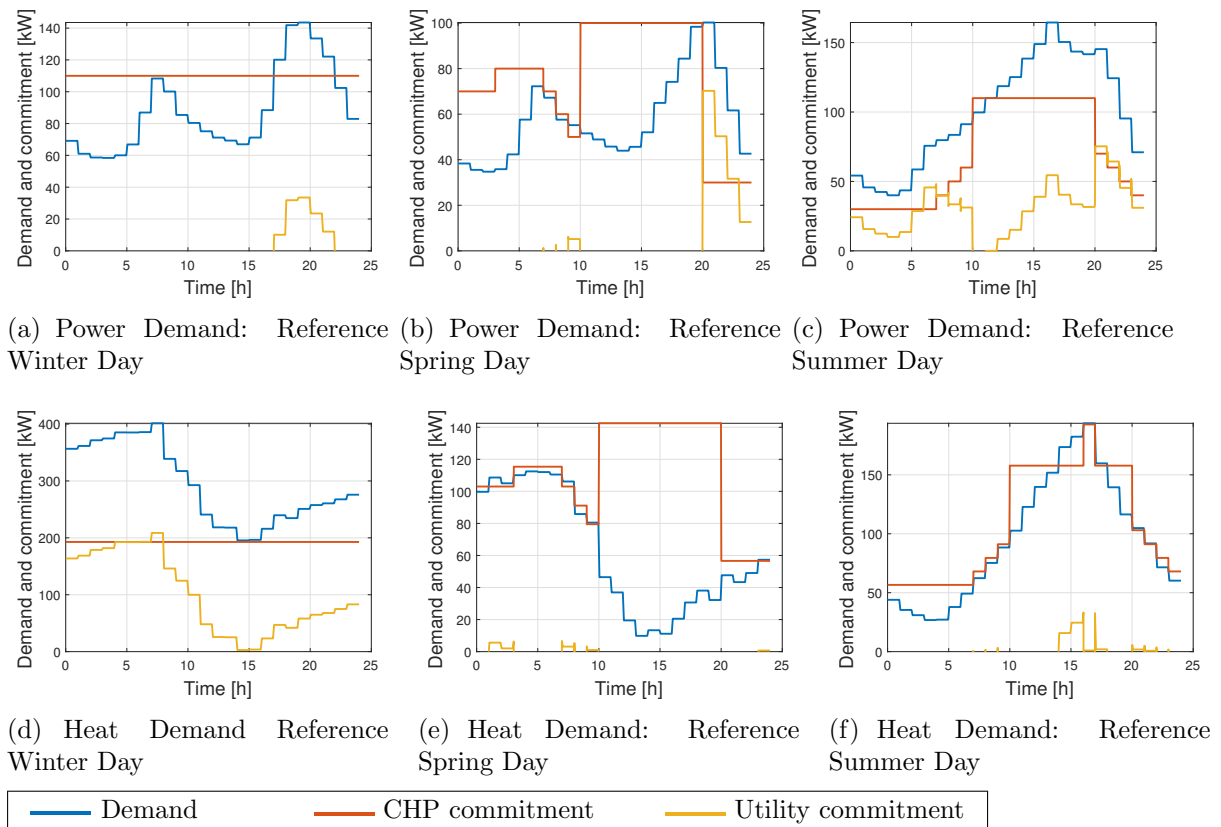


Figure 10: Heat and power demand of the residential community and its unit commitment solution for the seasonal reference days in winter, spring and summer.

C. Economic Analysis

To effectively demonstrate the economic viability of integrating the MGT, Table 4 summarizes the total savings when the natural gas price moderately deviates from the October 2015 reference of fuel cost 1= $\$7.74/1000ft^3$ to fuel cost 2 = $\$8.85/1000ft^3$ and fuel cost 3 = $\$6.80/1000ft^3$ [60]. Simulations for different building types were also performed for comparison. The results are aggregated by day (Summer, Spring/Autumn, Winter) and

building types. If the savings are listed as zero, it is not economically beneficial to operate the CHP unit. To facilitate the analysis, the data is further broken down to show the demand charge savings, Table 5 (which are divided by 30 as the usual billing period is one month).

Table 4: Absolute daily savings, for all buildings, days and fuel cost combinations (\$)

	Full Service Restaurant			Small Hotel			Residential			Large Hotel		
Fuel Cost (\$/1000ft ³)	7.74	8.85	6.80	7.74	8.85	6.80	7.74	8.85	6.80	7.74	8.85	6.80
Winter Day	22.66	16.82	27.76	12.00	8.07	16.86	97.17	88.40	105.21	58.78	49.62	66.03
Spring Day	0.00	0.00	0.00	0.00	0.00	0.00	37.85	26.90	48.58	58.74	49.60	66.00
Summer Day	0.00	0.00	0.00	67.40	0.00	87.26	241.32	233.42	248.27	150.27	141.97	159.10

Table 5: Daily demand charging savings, for all buildings, days and fuel cost combinations (\$)

	Full Service Restaurant			Small Hotel			Residential			Large Hotel		
Fuel Cost (\$/1000ft ³)	7.74	8.85	6.80	7.74	8.85	6.80	7.74	8.85	6.80	7.74	8.85	6.80
Winter Day	Peak	0.00	0.00	0.00	0.00	0.00	0.00	0.00	0.00	0.00	0.00	0.00
	Intermediate	7.80	7.80	7.80	3.98	3.98	5.28	0.00	0.00	19.58	17.80	19.58
Spring Day	Peak	0.00	0.00	0.00	0.00	0.00	0.00	0.00	0.00	0.00	0.00	0.00
	Intermediate	0.00	0.00	0.00	0.00	0.00	0.00	0.00	0.00	19.58	17.80	19.58
Summer Day	Peak	0.00	0.00	0.00	60.64	0.00	75.80	0.00	0.00	82.28	82.28	74.80
	Intermediate	0.00	0.00	0.00	5.20	0.00	5.88	0.00	0.00	19.58	14.25	19.58

For the commercial tall and medium buildings, there are savings resulting from fixed pricing of electricity and demand charge reduction (Table 5). The latter is associated with operating the unit at a nearly constant commitment level that decreases the peak loads met by the utility. For these reasons, in the large hotel example, using a single CHP unit is especially advantageous (Table 4), however insufficient in terms of meeting demand. Therefore, a bank of CHP units may be more suitable to accommodate the energy needs. In general for all commercial buildings, increasing the fuel price leads to a decrease in savings. This is most clearly demonstrated in the small hotel, where increasing the fuel price renders the unit economically inoperable.

The largest savings are observed for the residential neighborhood (Table 4), despite the tariff which excludes demand charges (hence, the corresponding entries in Table 5 are null). All the savings stem from the fixed pricing of energy and revenue generation. Assuming that a CHP unit is associated with a fixed cost of investment of $\sim \$150k$, the return on investment for the residential neighborhood occurs in ~ 3.27 years, based on a daily estimated saving of \$125.47 (average of the three days for the regular fuel price).

V. Conclusion

A comprehensive micro-gas turbine model was established for the purpose of optimizing the operational behavior of a CHP unit in a smart-grid environment. Real demand profiles and existing electricity tariffs were used to an accurate optimization model for solving the economic dispatch problem of an MGT unit under CHP operation. The unit commitment problem was then solved for four different typical consumers on rep-

representative days from all seasons. Of main interest is the observation that the optimal solution results in four distinct MGT operation modes: electricity driven, heat driven, maintenance cost driven, and revenue driven. In all the case studies, the integration of a micro-gas turbine as a CHP unit in a smart grid setting leads to significant economic benefits.

References

- [1] P. Criqui, *Prospective Outlook on Long-term Energy Systems: EUR 17358 EN*, Bruselas, 1996.
- [2] “Eu energy in figures: Statistical pocketbook 2015,” Luxembourg, 2015.
- [3] U.S. Energy Information Administration, “Annual energy outlook 2015,” <http://www.eia.gov/forecasts/aeo/>.
- [4] “Eu energy, transport and ghg emissions: Trends to 2050 : reference scenario 2013,” Luxembourg, 2014.
- [5] P. A. Pilavachi, “Mini- and micro-gas turbines for combined heat and power,” *Applied Thermal Engineering*, vol. 22, no. 18, pp. 2003–2014, 2002.
- [6] Ackermann, T., G. Andersson, and L. Söder, “Distributed generation: a definition,” *Electric power systems research*, no. 3, pp. 195–204, 2001.
- [7] A. Buonomano, F. Calise, M. D. D’Accadia, A. Palombo, and M. Vicidomini, “Hybrid solid oxide fuel cells-gas turbine systems for combined heat and power: A review,” *Applied Energy*, vol. 156, pp. 32–85, 2015.
- [8] P. Crespo Del Granado, Z. Pang, and S. W. Wallace, “Synergy of smart grids and hybrid distributed generation on the value of energy storage,” *Applied Energy*, vol. 170, pp. 476–488, 2016.
- [9] J. Peirs, T. Waumans, P. Vleugels, F. Al-Bender, T. Stevens, T. Verstraete, S. Stevens, R. D’hulst, D. Verstraete, P. Fiorini, R. van den Braembussche, J. Driesen, R. Puers, P. Hendrick, M. Baelmans, and D. Reynaerts, “Micropower generation with microturbines: a challenge,” *Proceedings of the Institution of Mechanical Engineers, Part C: Journal of Mechanical Engineering Science*, vol. 221, no. 4, pp. 489–500, 2007.
- [10] N. Lymberopoulos, “Microturbines and their application in bio-energy: Eesd contract no: Nne5-pta-2002-003/1,” 2004.
- [11] M. W. Davis, “Mini gas turbines and high speed generators a preferred choice for serving large commercial customers and microgrids. i. generating system,” in *Power Engineering Society Summer Meeting, 2002 IEEE*, vol. 2, July 2002, pp. 669–676.
- [12] E. Logan Jr, *Handbook of turbomachinery*. CRC Press, 2003.
- [13] T. Giampaolo, *The gas turbine handbook: Principles and practices*. CRC Press, 2003.

- [14] Walsh, P.P. and P. Fletcher, *Gas turbine performance*, John Wiley & Sons, 2004.
- [15] R. J. Yinger, "Behavior of Capstone and Honeywell microturbine generators during load changes," *Lawrence Berkeley National Laboratory*, no. February, p. 38, 2001.
- [16] E. Merkel, R. McKenna, and W. Fichtner, "Optimisation of the capacity and the dispatch of decentralised micro-CHP systems: A case study for the UK," *Applied Energy*, vol. 140, pp. 120–134, 2015.
- [17] C. R. Touretzky, D. L. McGuffin, J. C. Ziesmer, and M. Baldea, "The effect of distributed electricity generation using natural gas on the electric and natural gas grids," *Applied Energy*, vol. 177, pp. 500–514, 2016.
- [18] H. Wang, W. Yin, E. Abdollahi, R. Lahdelma, and W. Jiao, "Modelling and optimization of CHP based district heating system with renewable energy production and energy storage," *Applied Energy*, vol. 159, pp. 401–421, 2015.
- [19] M. A. Ehyaei and M. N. Bahadori, "Selection of micro turbines to meet electrical and thermal energy needs of residential buildings in Iran," *Energy & Buildings*, vol. 39, pp. 1227–1234, 2007.
- [20] F. Basrawi and T. Yamada, "Theoretical analysis of performance of a micro gas turbine co/trigeneration system for residential buildings in a tropical region," *Energy & Buildings*, vol. 67, pp. 108–117, 2013.
- [21] H. Ren and W. Gao, "Economic and environmental evaluation of micro CHP systems with different operating modes for residential buildings in Japan," *Energy & Buildings*, vol. 42, no. 6, pp. 853–861, 2010.
- [22] M. Ebrahimi and A. Keshavarz, "Prime mover selection for a residential micro-CCHP by using two multi-criteria decision-making methods," *Energy & Buildings*, vol. 55, pp. 322–331, 2012.
- [23] L. K. Kirchmayer, *Economic Operation of Power Systems*. New York: John Wiley & Sons, Inc., 1958.
- [24] J. Muckstadt and S. Koenig, "An Application of Lagrangian Relaxation to Scheduling in Power Generation Systems," *Operations Research*, vol. 25, no. 3, pp. 387–403, 1977.
- [25] X. Guan, P. Luh, H. Yan, and J. Amalfi, "An optimization-based method for unit commitment," *Electrical Power & Energy Systems*, vol. 14, no. 1, pp. 9–17, 1992.
- [26] G. Díaz and B. Moreno, "Valuation under uncertain energy prices and load demands of micro-CHP plants supplemented by optimally switched thermal energy storage," *Applied Energy*, vol. 177, pp. 553–569, 2016.
- [27] L. Galanti and A. F. Massardo, "Micro gas turbine thermodynamic and economic analysis up to 500kwe size," *Applied energy*, vol. 88, no. 12, pp. 4795–4802, 2011.
- [28] A. Al-Hinai and A. Feliachi, "Dynamic model of a microturbine used as a distributed generator," in *System Theory, 2002. Proceedings of the Thirty-Fourth Southeastern Symposium on*. IEEE, 2002, pp. 209–213.

- [29] R. Lasseter, "Dynamic models for micro-turbines and fuel cells," in *Power Engineering Society Summer Meeting, 2001*, vol. 2. IEEE, 2001, pp. 761–766.
- [30] L. N. Hannett, G. Jee, and B. Fardanesh, "A governor/turbine model for a twin-shaft combustion turbine," *IEEE Transactions on Power Systems*, vol. 10, no. 1, pp. 133–140, 1995.
- [31] L. Hannett and A. Khan, "Combustion turbine dynamic model validation from tests," *IEEE Transactions on Power Systems*, vol. 8, no. 1, pp. 152–158, 1993.
- [32] F. Sellers and J. Carl, "Dyngen - a program for calculating steady-state and transient performance of turbojet and turbofan engines," vol. NASA TN D-, no. April, 1975.
- [33] H. I. H. Saravanamuttoo, H. Cohen, and G. F. C. Rogers, *Gas turbine theory*, 5th ed. Harlow, England and New York: Prentice Hall, 2001.
- [34] H.-W. D. Chiang, C.-N. Hsu, A. Lai, and R. Lin, "An investigation of steady and dynamic performance of a small turbojet engine," in *ASME Turbo Expo 2002: Power for Land, Sea, and Air*. American Society of Mechanical Engineers, 2002, pp. 1097–1104.
- [35] "Ansaldo energia homepage," <http://www.ansaldoenergia.it/>.
- [36] "Capstone turbine corporation homepage," <http://www.capstoneturbine.com/>.
- [37] "Durr cleantechology homepage," <http://www.durr-cleantechology.com/>.
- [38] "La micro-cogenerazione a gas naturale: una nuova via del risparmio energetico: Sileo, m." http://www.ambientediritto.it/dottrina/Politiche%20energetiche%20ambientali/politiche%20e.a/micro_cogenerazione_sileo.htm.
- [39] Ingersoll-Rand Energy Systems, "Test and Quality Assurance Plan - IR Power Works - 70kW Microturbine System, SRI/USEPA-GHG-QAP-21," 202.
- [40] ——, "ETV Joint Verification Statement, SRI/USEPA-VS-GHG-VR-21," pp. 1–6, 2003.
- [41] A. Jones, "Npt-171 turbojet performance prediction method," *Noel Penny Turbine Ltd., internal publication*, pp. 2–21, 1983.
- [42] "Hx cpt 95-9-0 gas turbine heat recuperator," <http://www.acte-sa.be/>, 2015-03.
- [43] "Waste heat recovery: Technology and opportunities in the u.s. industry," http://www1.eere.energy.gov/manufacturing/intensiveprocesses/pdfs/waste_heat_recovery.pdf.
- [44] C. Kren, "Flue gas fired absorption chillers," Dissertation, München, 2006.
- [45] "Waste heat integration of electrical power generation provided by fuel cells," <http://epb.lbl.gov/thermal/waste.html>.

- [46] Advanced Manufacturing Office, “Use low-grade waste steam to power absorption chillers: Energy tips: Steam,” https://www1.eere.energy.gov/manufacturing/tech-assistance/pdfs/steam14_chillers.pdf, 2012.
- [47] Kadosh, K., Cukurel, B., “Micro-turbojet to turbofan conversion via continuously variable transmission: Thermodynamic performance study,” in *ASME Turbo Expo 2016*, pp. GT2016–56 274.
- [48] D. Zelazo, R. Dai, and M. Mesbahi, “An energy management system for off-grid power systems,” *Energy Systems*, vol. 3, no. 2, pp. 153–179, 2012.
- [49] D. P. Bertsekas, *Dynamic programming and optimal control*, 3rd ed., ser. Athena scientific optimization and computation series. Belmont, Mass.: Athena Scientific, 2007, vol. 3.
- [50] T. H. Cormen, C. Stein, R. L. Rivest, and C. E. Leiserson, *Introduction to Algorithms*, 2nd ed. McGraw-Hill Higher Education, 2001.
- [51] A. B. Kahn, “Topological sorting of large networks,” *Communications of the ACM*, vol. 5, no. 11, pp. 558–562, Nov. 1962.
- [52] S. Majumdar, “Low-cycle fatigue and creep analysis of gas turbine engine components,” *Journal of Aircraft*, vol. 12, no. 4, pp. 376–382, 1975.
- [53] “Commercial reference buildings,” <http://energy.gov/eere/buildings/commercial-reference-buildings>.
- [54] “Building characteristics for residential hourly load data: Based on building america house simulation protocols,” <http://en.openei.org/doe-opendata/dataset/eadfdbd10-67a2-4f64-a394-3176c7b686c1/resource/cd6704ba-3f53-4632-8d08-c9597842fde3/download/buildingcharacteristicsforresidentialhourlyloaddata.pdf>, 2010.
- [55] M. Beaudin, H. Zareipour, and A. Schellenberg, “A framework for modelling residential prosumption devices and electricity tariffs for residential demand response,” pp. 1–8, 2014.
- [56] PSEG LINY, “Tariff for electric service residential,” https://www.psegliny.com/files.cfm/rates_resi.pdf, New York, 2016.
- [57] ——, “Tariff for electric service commercial,” 2016.
- [58] ——, “How to read your bill,” <https://www.psegliny.com/page.cfm/Commercial/Account/MyBill/ReadBill>, 2016-9.
- [59] I. A. Sajjad, M. Manganelli, L. Martirano, R. Napoli, G. Chicco, and G. Parise, “Net metering benefits for residential buildings: A case study in italy,” in *IEEE 15th International Conference on Environment and Electrical Engineering (EEEIC)*, 2015, pp. 1647–1652.
- [60] U.S. Energy Information Administration, “U.S. Natural Gas Prices,” https://www.eia.gov/dnav/ng/ng_pri_sum_dcu_nus_a.htm, 2016.